



1 **Correct boundary conditions for DNS models of**
2 **nonlinear acoustic-gravity waves forced by**
3 **atmospheric pressure variations.**
4

5 **Yuliya Kurdyeva¹, Sergey Kshevetskii¹, Nikolai Gavrilov², Sergey Kulichkov³**
6

7 [1]{ Baltic Federal University, Institute of Physical-Mathematical Sciences and Information
8 Technologies, Kaliningrad, Russia }

9 [2]{Saint-Petersburg State University, Atmospheric Physics Department, Russia}

10 [3]{ Obukhov Institute of Atmospheric Physics, Russian Academy of Science, Moscow, Russia}

11 Correspondence to S. P. Kshevetskii (spkshev@gmail.com)
12

13 **Abstract**

14 Currently, international networks exist for high-resolution microbarograph recording wave
15 pressure variations at the surface of the Earth. This increases interest in simulating propagation
16 of waves caused by variations of atmospheric pressure. Such mathematical problem involves a
17 set of primitive nonlinear hydrodynamic equations with lower boundary conditions in the form
18 of wavelike pressure variations at the Earth's surface. To analyze the correctness of the problem,
19 the linearized equations are used near the ground for small amplitudes of surface wave
20 excitation. The method of wave energy functional shows that in nondissipative approximation
21 the solution of the boundary problem is uniquely determined by the variable pressure field at the
22 Earth's surface. Respective dissipative problem has also unique solution with the appropriate
23 choice of lower boundary conditions for temperature and velocity components. To test the
24 numerical algorithm, analytical solutions of the linearized equations for acoustic and gravity
25 wave modes are used. Reasonable agreements of numerical and analytical solutions are obtained.
26 Analytical studies show possibilities of sharp changes of temperature and density near the
27 ground. Numerical simulations confirm these analytical results. Obtained algorithms and
28 computer codes can be used for simulations of atmospheric wave propagation from the pressure
29 variations at the Earth's surface.

30 **1 Introduction**

31 Acoustic-gravity waves (AGWs) are observed in the atmosphere almost permanently.
32 According to recent knowledge, atmospheric AGWs propagating in the middle and upper
33 atmosphere can be excited at tropospheric heights. These waves can be generated by mesoscale



1 turbulence and convection (Fritts and Alexander, 2003; Fritts et al., 2006), atmospheric fronts
2 and jet streams (e.g., Gavrilov and Fukao, 1999; Plougonven and Snyder, 2007; Plougonven and
3 Zhang, 2014;) with maximum wave excitation efficiency at altitudes 9-12 km (e.g., Medvedev
4 and Gavrilov, 1995; Dalin et al., 2016). Generated waves can propagate from tropospheric
5 heights to the middle and upper atmosphere, where they can break and produce turbulence, or
6 other instability events (e.g., Fritts and Alexander, 2003; Gavrilov and Yudin, 1992; Gavrilov
7 and Fukao, 1999). AGW appearance is often associated with meteorological phenomena (Blanc
8 et al., 2014). During the origin and evolution of Cumulus clouds, water phase transitions and
9 respective heating/cooling occur, which can produce substantial generation of wave processes in
10 the atmosphere (e.g., Pierce and Coroniti, 1966; Balachandran, 1980; Fovell et al., 1992; Miller,
11 1999; Alexander et al., 2004; Blanc et al., 2014).

12 To simulate atmospheric AGWs and turbulence, numerical models based on non-
13 hydrostatic primitive hydrodynamic equations are recently used. Baker and Schubert (2000)
14 simulated distribution of nonlinear waves in the atmosphere of Venus, using the localized area
15 with horizontal and vertical dimensions of 120 km and 48 km, respectively. Fritts and Garten
16 (1996) and Andreassen et al. (1998) simulated Kelvin-Helmholtz instability and turbulence
17 generation by breaking waves. They used atmospheric areas with relatively small vertical and
18 horizontal dimensions, and applied Halerkin-type algorithms, based on the conversion of initial
19 hydrodynamic equations into sets of equations for spectral components. Yu et al. (2009) and Liu
20 et al. (2008) developed two-dimensional numerical models for propagating atmospheric AGWs.

21 Gavrilov and Kshevetskii (2013, 2015) developed two-dimensional numerical methods
22 for high-resolution wave simulation based on hydrodynamic conservation laws. Such numerical
23 methods ensuring precise execution of basic conservation laws are called as conservative. These
24 methods allow simulating even processes, in which solutions of nonlinear hydrodynamic
25 equations can be non-smooth. Such solutions are called as generalized or weak solutions of
26 hydrodynamic equations. Requirements of accurate holding fundamental conservation laws are
27 important for these methods, because they allow obtaining physically reasonable generalized
28 solutions to the equations. The basic ideas of the generalized solution theory and respective
29 numerical techniques were formulated by Lax (1957) and Lax and Wendroff (1960). Kshevetskii
30 (2001b, c), also Kshevetskii and Gavrilov (2003) developed stable two-dimensional AGW
31 algorithms and models. Gavrilov and Kshevetskii (2014a) extended their two-dimensional model
32 to the three-dimensional version. They used this 3D model to simulate AGW propagation from
33 the harmonic forcing at the Earth's surface.



1 Kshevetskii and Kulichkov (2015) used a three-dimensional nonlinear model for
2 description of the AGW generation by heating/cooling atmospheric gas in water phase
3 transitions during evolutions of thunderstorm clouds. Particularly, they studied connections of
4 local atmospheric pressure with the formation and development of thundercloud, and simulated
5 AGW propagation to the middle and upper atmosphere. Karpov and Kshevetskii (2014) modeled
6 AGW propagation from the local non-stationary source located at the Earth's surface. They
7 showed that infrasound waves propagating from tropospheric heights could significantly heat the
8 upper atmosphere. In addition, decaying waves can create jet streams currents in the upper
9 atmosphere. These effects require further detailed studies because of great diversity of their
10 characteristics. Processes of Cumulus cloud evolution lead to AGW generation (e.g., Blanc et al.,
11 2014; Alexander et al., 2004). These waves can reach the Earth's surface and can change the
12 surface pressure (Blanc et al., 2014; Kshevetskii and Kulichkov, 2015).

13 Regardless the reasons leading to wave variations of the surface pressure, one can use
14 these variations the lower boundary conditions for AGW simulations in the atmosphere. Wave
15 variations of the atmospheric surface pressure are recorded with microbarographs. Networks of
16 microbarographs exist and actively expanded currently in Europe and Africa (Blanc et al., 2014).
17 It is tempting to use this experimental data for AGW simulating in the atmosphere. However, the
18 specifying the surface pressure as lower boundary conditions in the nonlinear numerical AGW
19 models raise some problems not adequately studied in the past. In the present paper, we are
20 going to discuss these problems and consider methods for their solutions.

21 First, we perform a mathematical analysis of a set of primitive hydrodynamic equations
22 in order to offer the correct formulating the mathematical problem about propagation of AGWs
23 forced by pressure variations at the lower boundary of the atmosphere. Nonlinear equations are
24 difficult for strict mathematical analysis. However, wave amplitudes at the Earth's surface are
25 usually small. This allows starting the correctness study from the analysis of linearized
26 equations. Hydrodynamic equations contain atmospheric density and temperature. For zero
27 vertical speed of the Earth's surface, numerical methods require setting the temperature and
28 density at the lower boundary of the atmosphere. However, we found below that the solution of
29 the boundary problem is uniquely identified by specifying a variable pressure field at the lower
30 boundary. This fact is not trivial and allows us correct simulating AGW propagation forced by
31 surface pressure variations.

32 We modified the high-resolution numerical AGW model described by Gavrilov and
33 Kshevetskii (2014a,b) and Gavrilov et al. (2015), and available online (ATMOSYM, 2016). The
34 model was adapted for simulating AGW propagation from varying surface pressure. We



1 performed test simulations and compared numerical results with exact analytical solutions
 2 obtained for respective linearized hydrodynamic equations. In addition, we made three-
 3 dimensional nonlinear simulation of AGWs caused by experimentally observed variations of
 4 atmospheric pressure at the Earth's surface.

5 **2 Numerical model**

6 In the present paper, we mainly consider the three-dimensional high-resolution numerical
 7 model ATMOSYM simulating atmospheric AGWs, which was developed by Gavrilov and
 8 Kshevetskii (2014a,b) and Gavrilov et al. (2015). Recently this model becomes available for all
 9 users online (see ATMOSYM, 2016)

10 **2.1 Nonlinear hydrodynamic equations.**

11 The ATMOSYM numerical model uses the following set of primitive hydrodynamic
 12 equations for the atmosphere considered as the ideal gas:

13 the continuity equation

$$14 \quad \frac{\partial \rho}{\partial t} + \frac{\partial \rho u}{\partial x} + \frac{\partial \rho v}{\partial y} + \frac{\partial \rho w}{\partial z} = 0; \quad (1)$$

15 the motion equations

$$16 \quad \frac{\partial \rho u}{\partial t} + \frac{\partial \rho u^2}{\partial x} + \frac{\partial \rho uv}{\partial y} + \frac{\partial \rho uw}{\partial z} + 2\rho \omega_z v = -\frac{\partial p}{\partial x} + \left(\frac{\partial^2}{\partial x^2} + \frac{\partial^2}{\partial y^2} \right) \zeta(z) u + \frac{\partial}{\partial z} \zeta(z) \frac{\partial u}{\partial z};$$

$$17 \quad \frac{\partial \rho v}{\partial t} + \frac{\partial \rho uv}{\partial x} + \frac{\partial \rho v^2}{\partial y} + \frac{\partial \rho vw}{\partial z} - 2\rho \omega_z u = -\frac{\partial p}{\partial y} + \left(\frac{\partial^2}{\partial x^2} + \frac{\partial^2}{\partial y^2} \right) \zeta(z) v + \frac{\partial}{\partial z} \zeta(z) \frac{\partial v}{\partial z}; \quad (2)$$

$$18 \quad \frac{\partial \rho w}{\partial t} + \frac{\partial \rho uw}{\partial x} + \frac{\partial \rho vw}{\partial y} + \frac{\partial \rho w^2}{\partial z} = -\frac{\partial p}{\partial z} - \rho g + \left(\frac{\partial^2}{\partial x^2} + \frac{\partial^2}{\partial y^2} \right) \zeta(z) w + \frac{\partial}{\partial z} \zeta(z) \frac{\partial w}{\partial z};$$

19 the heat balance equation

$$20 \quad \frac{1}{\gamma - 1} \left(\frac{\partial p}{\partial t} + \frac{\partial \rho u}{\partial x} + \frac{\partial \rho v}{\partial y} + \frac{\partial \rho w}{\partial z} \right) = -p \left(\frac{\partial u}{\partial x} + \frac{\partial v}{\partial y} + \frac{\partial w}{\partial z} \right) + \left(\frac{\partial^2}{\partial x^2} + \frac{\partial^2}{\partial y^2} \right) \kappa(z) T + \frac{\partial}{\partial z} \kappa(z) \frac{\partial (T')}{\partial z} + Q_{visc};$$

$$21 \quad Q_{visc} = \zeta(z) \left[\left(\frac{\partial u}{\partial x} \right)^2 + \left(\frac{\partial u}{\partial y} \right)^2 + \left(\frac{\partial u}{\partial z} \right)^2 + \left(\frac{\partial v}{\partial x} \right)^2 + \left(\frac{\partial v}{\partial y} \right)^2 + \left(\frac{\partial v}{\partial z} \right)^2 + \left(\frac{\partial w}{\partial x} \right)^2 + \left(\frac{\partial w}{\partial y} \right)^2 + \left(\frac{\partial w}{\partial z} \right)^2 \right]; \quad (3)$$

22 the ideal gas state equation

$$23 \quad p = \rho R_g T / \mu \quad (4)$$



1 In Eq. (1) – (4) t is time; x, y, z and u, v, w are coordinates and velocity components
2 directed, respectively, eastwards, northwards and upwards; p, ρ, T are pressure, density and
3 temperature; R_g is the universal gas constant; μ is the air molecular weight; g is the acceleration
4 of gravity; γ is the heat capacity ratio; ζ and κ are the dynamic viscosity and thermal conductivity
5 coefficients; ω_z is the vertical component of the angular velocity of the Earth's rotation.

6 Eq. (1) – (4) take into account non-linear and dissipative processes accompanying wave
7 propagation. They can describe, in particular, such complex phenomena as the formation of
8 shock waves, the wave breaking and turbulence generation. The AGWSYM numerical model
9 provides a self-consistent description of wave processes and takes into account the changes in
10 atmospheric parameters due to energy transfer from dissipating waves to the atmosphere.

11 Vertical profiles of the background temperature $T_0(z)$ are taken from the semi-empirical
12 atmospheric models NRL-MSISE-00 (Picone et al., 2002). Molecular kinematic viscosity is
13 approximated with the formula by Banks and Kokarts (1973):

14

$$15 \quad \nu_0(z) = \zeta_0(z) / \rho_0(z) = 3.4 \times 10^{-7} T_0(z) / \rho_0(z) \quad (5)$$

16

17 The molecular thermal conductivity coefficient is obtained with dividing the coefficient of
18 viscosity by the Prandtl number. Similar expressions for molecular viscosity and thermal
19 conductivity were used by Yu et al. (2009) and Liu et al. (2010). The ATMOSYM model also
20 takes into account vertical profiles of the background turbulent viscosity and thermal
21 conductivity with maxima about $10 \text{ m}^2 \text{ s}^{-1}$ near the ground and at altitude of 100 km, and a
22 minimum of $0.1 \text{ m}^2 \text{ s}^{-1}$ in the stratosphere (see Gavrilov, 2013). Model does not take into account
23 some effects (e.g., the dissipation due to ion friction and radiative heat exchange), which are less
24 important for high frequency AGV.

25 **2.2 Boundary conditions**

26 The ATMOSYM model simulates waves in a limited atmospheric region. For analyzing
27 spectral AGW components, periodical conditions at horizontal boundaries are frequently
28 appropriate. Let L_x and L_y are dimensions of the model area along axes x and y , respectively.
29 Then periodical horizontal boundary conditions have the following form:



$$\begin{aligned}
 u(x = L_x, y, z, t) &= u(x = 0, y, z, t), & u(x, y = L_y, z, t) &= u(x, y = 0, z, t), \\
 v(x = L_x, y, z, t) &= v(x = 0, y, z, t), & v(x, y = L_y, z, t) &= v(x, y = 0, z, t), \\
 w(x = L_x, y, z, t) &= w(x = 0, y, z, t), & w(x, y = L_y, z, t) &= w(x, y = 0, z, t), \\
 p(x = L_x, y, z, t) &= p(x = 0, y, z, t), & p(x, y = L_y, z, t) &= p(x, y = 0, z, t), \\
 \rho(x = L_x, y, z, t) &= \rho(x = 0, y, z, t), & \rho(x, y = L_y, z, t) &= \rho(x, y = 0, z, t), \\
 T(x = L_x, y, z, t) &= T(x = 0, y, z, t), & T(x, y = L_y, z, t) &= T(x, y = 0, z, t).
 \end{aligned} \tag{6}$$

At the top, standard upper boundary conditions for wave propagation problems in the thermosphere are used:

$$\left. \frac{\partial T}{\partial z} \right|_{z=h} = 0, \quad \left. \frac{\partial u}{\partial z} \right|_{z=h} = 0, \quad \left. \frac{\partial v}{\partial z} \right|_{z=h} = 0, \quad w \Big|_{z=h} = 0. \tag{7}$$

These boundary conditions are usually valid at high molecular viscosity and thermal conduction at high altitudes ($h \geq 500$ km). The equation set (1) – (4) is difficult for strict analysis and most boundary conditions are obtained empirically from simulation practice. At the Earth’s surface, one can specify conditions for velocity components. Most frequently, the air non-flow through the surface is supposed, when $w(x,y,z=0,t) = 0$. However, for studies of waves from earthquakes or tsunami (Matsamura et al., 2011; Kherani et. al., 2012; Shinagawa et al., 2007) or vertical vibrations of gas caused by convection (Fovell et al., 1992; Snively and Pasko, 2003), and in some other cases, $w(x,y,z=0,t)$ is specified on the basis of experimental data or using general assumptions about considered phenomena. The condition of the air adhesion at the Earth’s surface is natural in the viscous model, when $u(x,y,z=0,t) = 0$ and $v(x,y,z=0,t) = 0$. In addition, one should specify the lower boundary conditions for relative variations of pressure, density and temperature

$$P = p'/p_0 = (p - p_0)/p_0, \quad R = \rho'/\rho_0 = (\rho - \rho_0)/\rho_0, \quad \Theta = T'/T_0 = (T - T_0)/T_0, \tag{8}$$

where primes denote inclinations of hydrodynamic fields from respective background values denoted with zero subscripts. In the present study, we consider the usage of the surface pressure measurements as the lower boundary condition, when

$$P(x, y, z = 0, t) = f_p(x, y, t), \tag{9}$$

where $f_p(x,y,t)$ is an approximation function to the surface measurement data. Changes in the boundary condition for the other hydrodynamic variables may lead to non-correct mathematical problems. Therefore, the proper options for getting correct mathematical boundary problems require consideration.

3 Correctness of the boundary problem

System of nonlinear equations (1) – (4) is complex and difficult for analysis. However,



1 near the Earth's surface wave amplitudes are usually very small. Nonlinear components have the
 2 second order in the solution expansion versus the small amplitude, while the linear terms have
 3 the first order. Therefore, one can simplify the equation by removing nonlinear terms (see
 4 Gossard and Hook, 1975).

5

6 **3.1 Correctness of linearized non-dissipative problem.**

7 The linearized equation set obtained from Eqs. (1) – (4) for the case of two spatial
 8 variables neglecting viscous and heat conduction terms can be represented in the following form
 9 (Kshevetskii, 2001a, 2002):

$$\begin{aligned}
 10 \quad & (\rho_0 R)_t + (\rho_0 u)_x + (\rho_0 w)_z = 0; \quad P = R + \Theta; \\
 11 \quad & (\rho_0 u)_t + (p_0 P)_x = 0; \quad (\rho_0 w)_t + (p_0 P)_z + \rho_0 g R = 0; \\
 12 \quad & (\rho_0 \Theta)_t - (\gamma - 1)(p_0 P)_t / \gamma + \rho_0 w N^2 / g = 0,
 \end{aligned} \tag{10}$$

13 where N is the Brunt-Vaisala frequency; subscripts t , x and z denote respective differentiation.
 14 Eq. (10) is obtained for zero background wind, because the wind is usually small near the
 15 ground. The case of inclusion of viscosity and thermal conductivity is discussed in the next
 16 section. Two-dimension equations are considered here for simplicity. The three-dimensional
 17 analysis is similar, but formulae are more bulky. In the two-dimension case, the Coriolis forces
 18 are omitted. The initial conditions correspond to the lack of motions at $t = 0$:

$$19 \quad u(x, z, t = 0) = 0, \quad w(x, z, t = 0) = 0, \quad R(x, z, t = 0) = 0, \quad \Theta(x, z, t = 0) = 0. \tag{11}$$

20 At horizontal boundaries, the two-dimension version of periodical conditions (6) is used. The
 21 upper boundary condition

$$22 \quad w(x, z=h, t) = 0 \tag{12}$$

23 corresponds to Eq. (7). At the lower boundary we impose the condition (10), which can be
 24 rewritten as

$$25 \quad P(x, z = 0, t) = [R(x, z = 0, t) + \Theta(x, z = 0, t)] = f_p(x, t). \tag{13}$$

26 The most important property of the correct solution is its uniqueness. In this respect, the following
 27 theorem can be formulated:

28 **Theorem 1.** *If a continuous solution of equations (10) with initial conditions (11) and*
 29 *boundary conditions (6), (12) and (13) exists, then it is unique.*



1 The proof of this theorem is given in the Appendix A. This theorem has a consequence.

2 **Consequence.** The Theorem 1 states that in non-dissipative case the solution is uniquely
 3 determined by the pressure variations (13) at the lower boundary, but not the surface
 4 distributions of relative variations of density R and temperature Θ . This means that arbitrary
 5 functions can be added to and subtracted from the surface distributions of R and Θ , but the
 6 solution will be the same as far as the sum $R + \Theta = P$ is the same at the surface.

7 This allows constructing solutions of linearized non-dissipative equations having jumps
 8 in R and Θ near the lower boundary $z = 0$. In nonlinear models, such jumps can produce
 9 instabilities and generate mathematical wave modes non-existing in the nature. Therefore,
 10 nonlinear models require specifying correct self-consistent lower boundary conditions for R and
 11 Θ in addition to the condition (13) to minimize influence of mathematical wave modes.

12 3.2 Correctness of linearized dissipative problem

13 Linearized set of hydrodynamic equations for the case of two spatial dimensions, taking into account the
 14 dissipative terms is as follows:

$$\begin{aligned}
 15 \quad & (\rho_0 R)_t + (\rho_0 u)_x + (\rho_0 w)_z = 0; \quad P = R + \Theta; \\
 16 \quad & (\rho_0 u)_t + (p_0 P)_x = [\zeta \zeta(z) u_{xx} + [\zeta \zeta(z) (w_z)_z]; \\
 17 \quad & (\rho_0 w)_t + (p_0 P)_z + \rho_0 g R = [\zeta \zeta(z) w_{xx} + [\zeta \zeta(z) (w_z)_z]; \\
 18 \quad & (\rho_0 \Theta)_t - (\gamma - 1)(p_0 P)_t / \gamma + \rho_0 w N^2 / g = (\gamma - 1)[(\kappa(\kappa_0 \Theta)_{xx} + (\kappa \kappa(z)_0 \Theta)_z)_z],
 \end{aligned}
 \tag{14}$$

19 Compliment the equations (15) with the initial conditions (12). According to (7), the upper
 20 boundary have the form of

$$21 \quad (T_0 \Theta)_z|_{z=h} = 0, \quad u_z|_{z=h} = 0, \quad w(z=h) = 0. \tag{15}$$

22 Analogous to the Appendix A, one can proof the following uniqueness theorem:

23 **Theorem 2.** *If a continuous solution exists for the equations (14) with initial conditions*
 24 *(11) and boundary conditions (6), (13), (15) and*

$$25 \quad u|_{z=0} = 0, \quad w_z|_{z=0} = 0, \quad \Theta|_{z=0} = 0, \tag{16}$$

26 *then it is unique.*

27 This theorem is proved in the Appendix B. The last boundary condition in (16) leads to
 28 the following lower boundary condition for density variations:

$$29 \quad R(x, z=0, t) = f_p(x, t) - \Theta(x, z=0, t). \tag{17}$$



1 This condition should be added to the lower boundary conditions (13) and (16), when one is
 2 going to specify nonzero variations of pressure at the Earth's boundary for studies of AGW
 3 propagation.

4 As far as AGW amplitudes are usually small near the ground, one should expect that the
 5 solutions of nonlinear and linearized equations should be close near the lower boundary.
 6 Therefore, in the present study we solve the following nonlinear AGW boundary problem: a) the
 7 equation set is (1) – (4); b) zero initial conditions like (11); c) the horizontal boundary conditions
 8 (6); d) the lower boundary conditions (9), (16) and (17).

9 **4 Comparisons of nonlinear and linearized models.**

10 To study the influence of the lower boundary condition, we made comparisons of
 11 simulations using the nonlinear equations (1) – (4) and boundary conditions listed at the end of
 12 section 2.1 with analytical solution of the respective linearized equations.

13 **4.1 Analytical solution of linearized equations.**

14 For the set of linearized equations (10) in isothermal ($T_0 = \text{const}$) background conditions
 15 the following stationary solution can be obtained using standard methods described by Gossard
 16 and Hook (1975) and Beer (1974):

$$\begin{aligned}
 u(x, z, t) &= C \frac{gH_0 e^{\alpha z} k \cos(S)}{\omega}, \quad S = kx + mz - \omega t, \\
 R(x, z, t) &= C e^{\alpha z} \left[\left(\frac{gH_0 k^2}{\omega^2} + \frac{mA}{\omega} \right) \sin(S) + \frac{(4m^2 H_0 B + 2A + B)}{4H_0 \omega} \cos(S) \right], \\
 \Theta(x, z, t) &= C e^{\alpha z} \left[\left(\frac{1 - gH_0 k^2}{\omega^2} - \frac{mA}{\omega} \right) \sin(S) - \frac{(4m^2 H_0 B + 2A + B)}{4H_0 \omega} \cos(S) \right], \\
 w(x, z, t) &= A(R + \Theta) + B \frac{\partial}{\partial z} (R + \Theta),
 \end{aligned} \tag{18}$$

18 where k and m are the horizontal and vertical wave numbers, respectively; ω is the wave
 19 frequency; $\alpha = (2H_0)^{-2}$, A and B are coefficients having the forms of

$$A = \frac{(\gamma - 2\gamma m^2 H_0^2 - 2)(\gamma g H_0 k^2 - \omega^2)}{m\omega(4 - 4\gamma + \gamma^2 + 4\gamma^2 m^2 H_0^2)}, \quad B = \frac{2(2 - \gamma)(\gamma g H_0 k^2 - \omega^2)}{m\omega(4 - 4\gamma + \gamma^2 + 4\gamma^2 m^2 H_0^2)} \tag{19}$$

21 Wave numbers k , m and frequency ω are connected by the dispersion equation

$$\omega^2 = \frac{1}{2} \gamma g H_0 (m^2 + k^2 + \alpha^2) \left(1 \pm \sqrt{1 - \frac{4k^2(\gamma - 1)}{\gamma^2 H_0^2 (m^2 + k^2 + \alpha^2)}} \right) \tag{20}$$



1 Here the signs + and - before the square root correspond to acoustic and internal gravity waves
2 (IGWs), respectively. In Eq. (18) – (20) upward directions of group velocity correspond to $m > 0$
3 for acoustic and $m < 0$ for internal gravity waves.

4 **4.2 Test simulations.**

5 Numerical simulations for comparisons with analytical solutions (18) – (20) are made
6 with the AGWSYM model using the three-dimension algorithms for solving Eq. (1) – (4)
7 developed by Gavrilov and Kshevetskii (2015). We use the initial conditions (11), conditions at
8 the horizontal boundaries (6) and at the upper boundary (7). At the lower boundary $z = 0$, we use
9 conditions (16) and specify the plane wave pressure variation:

$$10 \quad P(x, y, z = 0, t) = D \sin(kx + mz - \omega t), \quad (21)$$

11 where D is the surface amplitude. Relative density variations at the lower boundary are
12 calculated using Eq. (17). Previous simulations with the model (e.g., Gavrilov and Kshevetskii,
13 2015) showed the existence of a transition interval after initiating the boundary forcing at $t = 0$
14 before the solution comes to a quasi-stationary regime. In this regime, we can expect good
15 agreement between the numerical results and the analytical solution (18) - (20) with $C = D\omega^2$ at
16 low altitudes, where AGW amplitudes and molecular viscosity and heat conductivity are small.

17 Numerical results are obtained using the AGWSYM (2016) model for solving the
18 equation set (1) – (4) with initial conditions (11) and conditions (6) at the horizontal boundaries,
19 (7) at the upper boundary, also (16), (17), (21) at the lower boundary. In test runs the atmosphere
20 is isothermal with $H_0 = 8$ km. The wave forcing (21) is activated at $t = 0$. One should expect that
21 at low altitudes, where wave amplitudes and dissipation are small, numerical solutions would
22 tend to linear analytical solution (18) – (20) with increasing t .

23 Test simulations were made for isothermal atmosphere with $H_0 = 8$ km, $L_x = 10^3$ km, $k =$
24 $40\pi/L_x$. Frequencies are $\omega = \pi/60$ s⁻¹ for the acoustic wave mode and $\omega = \pi/1800$ s⁻¹ for the IGW
25 mode. To prevent substantial initial AGW pulse at the surface forcing activation, the lower
26 boundary condition (21) was multiplied by factor $q = 1 - \exp(-t/t_0)$ with $t_0 = 2$ min. This factor
27 gradually increases in time from 0 to 1 and the intensity of initial AGW pulse become smaller.

28 Figure 1 shows numerical and analytical temperature wave fields in the lower atmosphere
29 at different t for the acoustic and IGW modes. Similarities of the left and right panels in Figure 1
30 mean good agreement between nonlinear numerical and linear analytical solutions for small
31 amplitude non-dissipative AGWs. Figure 2 represents numerical solutions with better resolution near
32 the lower boundary. One can see transitions from zero boundary condition for temperature (16) to wave



1 fields corresponding simulated AGW. The transition is sharp within a few vertical grid spacing near the
2 ground.

3 **4.4 Simulation for observed local pressure variations.**

4 To test the numerical model for real data, we used a sample of the surface pressure
5 variations in time, $f(t)$, recorded with microbarograph at the Obukhov Institute of Atmospheric
6 Physics near Moscow (55.7 N, 37,6 E) on April 9, 2016 and shown in Figure 3. Assuming
7 localized near the measurement location (x_0, y_0) wave source, the lower boundary condition (13)
8 for surface pressure are taken in the following form:

$$9 \quad P(x, y, z = 0, t) = \exp[-((x - x_0)^2 + (y - y_0)^2) / d^2] f(t), \quad (22)$$

10 where d is the half-width of the wave source region. For present simulations we set $d = 2$ km.
11 Other initial and boundary conditions are the same as in section 4.3. Simulated temperature
12 fields for $t \approx 3$ min after the wave source activation are shown in the left panel of Figure 4. One
13 can see acoustic waves propagating from the source with amplitudes increasing with height.
14 These acoustic waves have not so high amplitudes because the pressure measurements of Figure
15 3 correspond to quiet meteorological conditions near the observation site. In addition, observed
16 variations of the surface pressure are relatively slow and generate mainly IGWs. Group speed of
17 IGWs is much smaller than the sound speed. Therefore, IGWs in Figure 4 are noticeable near the
18 wave source region. The right panel of Figure 4 is for $t \approx 13$ min and demonstrates inclined
19 petals. This is characteristic for IGWs propagating in the atmosphere from localized wave
20 sources.

21 **5 Conclusion**

22 In this study, we set up and mathematically investigated the problem of propagating
23 nonlinear acoustic-gravity waves produced by variable pressure at the surface of the Earth. We
24 also compared the results with analytical solutions of linear AGW theory.

25 Mathematical study showed that solutions of problem of AGW propagation from variable
26 density and temperature specified on the Earth's surface are uniquely identified by the pressure
27 on the Earth's surface, but do not depend on details of individual temperature and density
28 distributions. Numerically simulated acoustic and IGW modes excited by harmonic variations of
29 pressure at the Earth's surface confirmed the theoretical results.

30 The problem of waves propagating from a harmonic source specified at the lower boundary
31 border can be solved analytically in the case of isothermal atmosphere. We compared analytical



1 and numerical solutions and demonstrated good agreement between them. Such comparisons can
2 be used for validating numerical models of atmospheric AGWs.

3 Reasonable agreement of wave parameters calculated using numerical simulation and
4 analytical formulae can be considered as an indication of adequate description of wave processes
5 by the nonlinear numerical model. An example is shown of numerical solution of AGW
6 propagation from local variations in the surface atmospheric pressure. Model of direct numerical
7 simulation can be effective for simulating AGWs produced by variations of atmospheric pressure
8 and for testing and validation of simplified parameterizations of wave effects in the atmosphere.

9

10 **Computer code availability**

11 The computer code is available for free online simulations for all users (see ATMOSYM,
12 2016). The code can be distributed and used with the permission from the Immanuel Kant Baltic
13 Federal (the official owner of the code). Access to the fully functional demo-version of the
14 ATMOSYM computer code, which calculates the experiments described in the present paper,
15 can be granted on demand by request to Sergej Kshevtskii (spkshev@gmail.com) or Yulia
16 Kurdyaeva (kamenokamen@mail.ru). Any questions should be directed to the authors.

17

18 *Acknowledgements.* This work was partly supported by the Russian Basic Research Foundation
19 (grant 17-05-00574), by the Russian Scientific Foundation (grant 14-17-00685).

20

21 **References.**

22 Alexander, M., May, P. and Beres, J.: Gravity waves generated by convection in the Darwin area
23 during the Darwin Area Wave Experiment, *J. Geophys. Res.*, 109, D20S04, 1-11, 2004.

24 Andreassen, O., Hvidsten, O., Fritts, D., and Arendt, S.: Vorticity dynamics in a breaking internal
25 gravity wave, Part I Initial instability evolution, *J. Fluid. Mech.*, 367, 27-46, 1998.

26 ATMOSYM: A multi-scale atmosphere model from the Earth's surface up to 500 km,
27 <http://atmos.dev.awsmtek.com>, 2016 (last access 10.02.2017).

28 Baker, D. and Schubert, G.: Convectively generated internal gravity waves in the lower atmosphere
29 of Venus, Part II mean wind shear and wave-mean flow interaction, *J. Atmos. Sci.*, 57, 200-215,
30 2000.



- 1 Balachandran, N. K.: Gravity waves from thunderstorms, *Monthly weather rev.*, 108, 804-816,
2 1980.
- 3 Banks, P. M. and Kockarts, G.: *Aeronomy, Part B*, Elsevier, New York, 1973.
- 4 Beer, T.: *Atmospheric waves*, Adam Hilder, London, 1974.
- 5 Blanc, E., Farges, T., Le Pichon, A., and Heinrich, P.: Ten year observations of gravity waves from
6 thunderstorms in western Africa, *J. Geophys. Res. Atmos.*, 119, 6409-6418,
7 doi:10.1002/2013JD020499, 2014.
- 8 Dalin, P., Gavrilov, N., Pertsev, N., Perminov, V., Pogoreltsev, A., Shevchuk, N., Dubietis, A.,
9 Volger, P., Zalcik, M., Ling, A., Kulikov, S., Zadorozhny, A., Salakhutdinov and Grigorieva, I.:
10 A case study of long gravity wave crests in noctilucent clouds and their origin in the upper
11 tropospheric jet stream, *J. Geophys. Res. Atmos.*, 121, 14,102–14,116,
12 doi:10.1002/2016JD025422, 2016.
- 13 Fritts, D. C. and Alexander, M. J.: Gravity wave dynamics and effects in the middle atmosphere,
14 *Rev. Geophys.*, 41, 1003, doi:10.1029/2001RG000106, 2003.
- 15 Fritts, D. C. and Garton, J. F.: Wave breaking and transition to turbulence in stratified shear flows,
16 *J. Atmos. Sci.*, 53, 1057-1085, 1996.
- 17 Fritts, D. C., Vadas, S. L., Wan, K., and Werne, J. A.: Mean and variable forcing of the middle
18 atmosphere by gravity waves, *J. Atmos. Sol.-Terr. Phys.*, 68, 247-265, 2006
- 19 Fovell, R., Durran, D., Holton, J.R.: Numerical simulation of convectively generated stratospheric
20 gravity waves, *J. Atmos. Sci.*, v. 47, 1427-1442, 1992.
- 21 Gavrilov, N. M.: Estimates of turbulent diffusivities and energy dissipation rates from satellite
22 measurements of spectra of stratospheric refractivity perturbations, *Atmos. Chem. Phys.*, 13,
23 12107-12116, doi:10.5194/acp-13-12107-2013, 2013.
- 24 Gavrilov, N. M. and Fukao, S.: A comparison of seasonal variations of gravity wave intensity
25 observed by the MU radar with a theoretical model, *J. Atmos. Sci.*, 56, 3485-3494,
26 doi:10.1175/1520-0469(1999)056<3485:ACOSVO>2.0.CO;2, 1999.
- 27 Gavrilov, N. M. and Kshevetskii, S. P.: Numerical modeling of propagation of breaking nonlinear
28 acoustic-gravity waves from the lower to the upper atmosphere, *Adv. Space Res.*, 51, 1168-1174,
29 doi:10.1016/j.asr.2012.10.023, 2013.



- 1 Gavrilov, N. M. and Kshevetskii, S. P.: Numerical modeling of the propagation of nonlinear
2 acoustic-gravity waves in the middle and upper atmosphere. *Izvestiya, Atmos. Ocean. Phys.*, 50,
3 66-72, doi:10.1134/S0001433813050046, 2014a.
- 4 Gavrilov, N. M. and Kshevetskii, S. P.: Three-dimensional numerical simulation of nonlinear
5 acoustic-gravity wave propagation from the troposphere to the thermosphere, *Earth Planets
6 Space*, 66, 88, doi:10.1186/1880-5981-66-88, 2014b.
- 7 Gavrilov, N. M. and Kshevetskii, S. P.: Dynamical and thermal effects of nonsteady nonlinear
8 acoustic-gravity waves propagating from tropospheric sources to the upper atmosphere, *Adv.
9 Space Res.*, 55, doi:10.1016/j.asr.2015.01.033, 2015.
- 10 Gavrilov, N. M. and Yudin, V. A.: Model for coefficients of turbulence and effective Prandtl
11 number produced by breaking gravity waves in the upper atmosphere, *J. Geophys. Res.*, 97,
12 7619B-7624, doi:10.1029/92JD00185, 1992.
- 13 Gossard, E. E. and Hooke, W. H.: *Waves in the atmosphere*, Elsevier Sci. Publ. Co., Amsterdam-
14 Oxford-New York, 1975.
- 15 Karpov, I. V. and Kshevetskii, S. P.: Formation of large-scale disturbances in the upper atmosphere
16 caused by acoustic-gravity wave sources on the Earth's surface, *Geomag. Aeronomy*, 54(4), 553-
17 562, doi:10.1134/S0016793214040173, 2014.
- 18 Kherani, E.A., Lognonne P., Hebert H, Rolland, L., Astafyeva, E., Occhipinti, G., Coisson P.,
19 Walwer D. and de Paula, E.R.: Modelling of the total electronic content and magnetic field
20 anomalies generated by the 2011 Tohoku-OkI tsunami and associated acoustic-gravity waves,
21 *Geophys. J. Int.*, 191, 1049-1066, DOI: 10.1111/j.1365-246X.2012.05617.x, 2012.
- 22 Kshevetskii, S. P.: Modelling of propagation of internal gravity waves in gases, *Comp. Math.
23 Mathematic. Phys.*, 41, 295-310, 2001a.
- 24 Kshevetskii, S. P.: Analytical and numerical investigation of non-linear internal gravity waves,
25 *Nonlin. Proc. Geoph.*, 8, 37-53, 2001b.
- 26 Kshevetskii, S. P.: Numerical simulation of nonlinear internal gravity waves, *Comp. Math. Math.
27 Phys.*, 41, 1777-1791, 2001c.
- 28 Kshevetskii, S.P.: Internal gravity waves in non-exponentially density-stratified fluids. *Comput.
29 Math. Mathematic. Phys.*, 42(10), 1510-1521, 2002.
- 30 Kshevetskii, S. P. and Gavrilov, N. M.: Vertical propagation of nonlinear gravity waves and their
31 breaking in the atmosphere, *Geomagn. Aeronomy*, 43(1), 69-76, 2003.



- 1 Kshevetskii, S. P. and Gavrilov, N. M.: Vertical propagation, breaking and effects of nonlinear
2 gravity waves in the atmosphere, *J. Atmos. Sol.-Terr. Phys.*, 67, 1014-1030, 2005.
- 3 Kshevetskii, S. P. and Kulichkov, S. N.: Effects that Internal Gravity Waves from Convective
4 Clouds Have on Atmospheric Pressure and Spatial Temperature-Disturbance Distribution,
5 *Atmospheric and Oceanic Physics*, 51(1), 42-48, doi:10.1134/S0001433815010065, 2015.
- 6 Lax, P. D.: Hyperbolic systems of conservation laws, *Comm. Pure Appl. Math.*, 10, 537-566, 1957.
- 7 Lax, P. D. and Wendroff, B.: Hyperbolic systems of conservation laws, *Comm. Pure Appl. Math.*,
8 13, 217-237, 1960.
- 9 Liu, H.-L., Foster, B. T., Hagan, M. E., McInerney, J. M., Maute, A., Qian, L., Richmond, A. D.,
10 Roble, R. G., Solomon, S. C., Garcia, R. R., Kinnison, D., Marsh, D. R., Smith, A. K., Richter,
11 J., Sassi, F., and Oberheide, J.: Thermosphere extension of the whole atmosphere community
12 climate model, *J. Geophys. Res.*, 115, A12302, doi:10.1029/2010JA015586, 2010.
- 13 Liu, X., Xu, J., Liu, H.-L., and Ma, R.: Nonlinear interactions between gravity waves with different
14 wavelengths and diurnal tide, *J. Geophys. Res.*, 113, D08112, doi:10.1029/2007JD009136, 2008.
- 15 Matsumura, M., Saito, A., Iyemori, T.; Shinagawa, H.; Tsugawa, T.; Otsuka, Y.; Nishioka, M.;
16 Chen, C. H.: Numerical simulations of atmospheric waves excited by the 2011 off the Pacific
17 coast of Tohoku Earthquake. *Earth, Planets and Space*. 63:68. doi:10.5047/eps.2011.07.015,
18 2011.
- 19 Medvedev, A. S. and Gavrilov, N. M.: The nonlinear mechanism of gravity wave generation by
20 meteorological motions in the atmosphere, *J. Atmos. Terr. Phys.*, 57, 1221-1231, 1995.
- 21 Miller, D.V.: Thunderstorm induced gravity waves as a potential hazard to commercial aircraft.
22 American Meteorological Society 79th Annual conference, Windham Anatole Hotel, Dallas, TX,
23 January 10-15. Dallas: American Meteorological Society. 1999.
- 24 Picone, J.M., Hedin, A.E., Drob, D.P. and Aikin, A.C. : NRL-MSISE-00 Empirical Model of the
25 Atmosphere: Statistical Comparisons and Scientific Issues, *J. Geophys. Res.*, 107(A12),
26 doi:10.1029/2002JA009430, 2002.
- 27 Pierce, A. D. and Coroniti, S. C.: A mechanism for the generation of acoustic-gravity waves during
28 thunder-storm formation, *Nature*, 210, 1209-1210, doi 10.1038/2101209a0, 1966.
- 29 Plougonven, R. and Snyder, Ch.: Inertia-gravity waves spontaneously generated by jets and fronts.
30 Part I: Different baroclinic life cycles, *J. Atmos. Sci.*, 64, 2502-2520, 2007.



- 1 Plougonven, R. and Zhang, F. : Internal gravity waves from atmospheric jets and fronts, Rev.
 2 Geophys., 52, doi:10.1002/2012RG000419, 2014.
- 3 Shinagawa, H., Iyemori, T., Saito, S. and Maruyama, T. : A numerical simulation of
 4 ionospheric and atmospheric variations associated with the Sumatra earthquake on December 26,
 5 2004, Earth Planets Space, 59, 1015-1026, 2007.
- 6 Snively, J..B. and Pasko, V.B.: Breaking of thunderstorm generated gravity waves as a source of
 7 short period ducted waves at mesopause altitudes, Geophys. Res. Lett, v. 30, No 24, 2254,
 8 doi:10.1029/2003GL018436.,2003.
- 9 Yu, Y., Hickey, M. P., and Liu, Y.: A numerical model characterizing internal gravity wave
 10 propagation into the upper atmosphere, Adv. Space Res., 44, 836-846,
 11 doi:10.1016/j.asr.2009.05.014, 2009.

12

13 **Appendix A. Proof of the Theorem 1.**

14 The Theorem 1 formulated in section 3.1 for the linearized non-dissipative problem states
 15 that *if a continuous solution of equations (10) with initial conditions (11) and boundary*
 16 *conditions (6), (12), (13) exists, then it is unique.*

17 To proof of this uniqueness theorem one can use the indirect (“the proof by
 18 contradiction”) method. Suppose that two different solutions $\chi_1 = (u_1, w_1, P_1, \Pi_1, \Theta_1)$ and χ_2
 19 $= (u_2, w_2, P_2, \Pi_2, \Theta_2)$ exist. Consider the difference of these solutions: $\Delta\chi = (\tilde{u}, \tilde{w}, \tilde{P}, \tilde{\Pi}, \tilde{\Theta})$, where
 20 $\tilde{u} = u_1 - u_2$, $\tilde{w} = w_1 - w_2$, $\tilde{P} = P_1 - P_2$, $\tilde{\Pi} = \Pi_1 - \Pi_2$, $\tilde{\Theta} = \Theta_1 - \Theta_2$. If the function $f_p(x, t)$ in
 21 Eq. (13) is the same for both P_1 and P_2 , the difference $\Delta\chi$ satisfies to Eq. (10) with the initial
 22 conditions (11) and boundary conditions (6) and (12). The standard wave energy, e , balance for
 23 the Eq. (11) has the following differential form (Gossard and Hooke, 1975):

24

$$25 \quad \frac{\partial e}{\partial t} + \text{div} \vec{j} = 0; \quad \vec{j} = (p_0 P u, p_0 P w);$$

$$26 \quad e = \frac{1}{2} \rho_0 \left[(u^2 + w^2) + gH \left(\frac{P^2}{\gamma} + \frac{(\Pi - (\gamma - 1)\Theta)^2}{\gamma\alpha} \right) \right]. \quad (\text{A1.1})$$

26

27 This equation should be valid for the solution $\Delta\chi$ also. Put this solution to (A1.1) and integrate
 28 the obtained equation over the time-spatial domain $\Omega \times [0, t]$, where $\Omega = [0, L_x] \times [0, h]$ is the
 29 considered atmospheric area. Then one can apply the Gauss’s flux theorem, use the zero initial



1 conditions (11) and obtain the following relation:

2

$$\begin{aligned}
 & \frac{1}{2} \int_{\Omega} \rho_0 \left(\tilde{u}^2 + \tilde{w}^2 + gH \frac{\tilde{P}^2}{\gamma} + gH \frac{(\tilde{\Pi} - (\gamma - 1)\tilde{\Theta})^2}{\gamma\alpha} \right) d\Omega = \\
 & = - \int_0^t \int_S p_0 \tilde{P} \tilde{v} d\bar{S} dt, \quad \tilde{v} = (\tilde{u}, \tilde{v}).
 \end{aligned}
 \tag{A1.2}$$

3

4
 5 Here S is the boundary of the Ω region, $d\bar{S} = \bar{n} dS$, \bar{n} is the external vector, which is normal to
 6 the region boundary S . Integration circuit of S includes upper, horizontal and lower boundaries.

7 Consider the right side integral in Eq. (A1.2). Its part along the upper boundary $z = h$ is equal to
 8 zero due to the condition (12). Because of periodical conditions (6), the parts of the integral
 9 along the left and right boundaries ($x = 0$ and $x = L_x$) compensate each other, because they have
 10 the same absolute values, but opposite signs. For the lower boundary condition (13) with fixed
 11 $f_p(x, t)$ the difference $\tilde{P}(x, z = 0, t) = 0$ and the part of considered integral along the lower surface z
 12 $= 0$ is equal to zero.

13 Summarizing, one can see that the surface integral in the right part of Eq. (A1.2) is equal
 14 to zero for considered initial and boundary conditions. This means that all quantities marked with
 15 waves in the left part integral of Eq. (A1.2) should be zero, or that $\chi_1 \equiv \chi_2$.

16 Appendix B. Proof of the Theorem 2.

17 The Theorem 2 formulated in section 3.2 for linearized dissipative problem states that *if a*
 18 *continuous solution of equations (14) with initial conditions (11) and boundary conditions (6),*
 19 *(13), (15) and (16) exists, then it is unique.*

20 To proof this uniqueness theorem the standard indirect (“the proof by contradiction”) method similar to Appendix A can be used. Suppose again that two different solutions $\chi_1 = (u_1,$
 21 $w_1, P_1, \Pi_1, \Theta_1)$ and $\chi_2 = (u_2, w_2, P_2, \Pi_2, \Theta_2)$ exist. Consider the difference of these solutions:
 22 $\Delta\chi = (\tilde{u}, \tilde{w}, \tilde{P}, \tilde{\Pi}, \tilde{\Theta})$, where $\tilde{u} = u_1 - u_2$, $\tilde{w} = w_1 - w_2$, $\tilde{P} = P_1 - P_2$, $\tilde{\Pi} = \Pi_1 - \Pi_2$,
 23 $\tilde{\Theta} = \Theta_1 - \Theta_2$. Function $\Delta\chi$ satisfies Eq. (14) with initial conditions (11) and boundary conditions
 24 (6), (13), (15) and (16). Getting the wave energy equation for Eq. (14) and applying the Gauss’s
 25 flux theorem one can get the following equation similar to (A1.2):
 26

27



$$\begin{aligned}
 & \frac{1}{2} \int_{\Omega} \rho_0 \left(\tilde{u}^2 + \tilde{w}^2 + gH \frac{\tilde{P}^2}{\gamma} + gH \frac{(\tilde{\Pi} - (\gamma - 1)\tilde{\Theta})^2}{\gamma\alpha} \right) d\Omega + \\
 1 \quad & + \int_0^t \int_{\Omega} \left[\zeta ((\tilde{u}_x)^2 + (\tilde{u}_z)^2 + (\tilde{w}_x)^2 + (\tilde{w}_z)^2) + \kappa T_0 ((\tilde{\Theta}_x)^2 + (\tilde{\Theta}_z)^2) \right] d\Omega dt = \quad (A2.1) \\
 & = - \int_0^t \int_0^{L_z} \left[p_0 \tilde{P} \tilde{w} + \zeta (\tilde{u} \tilde{u}_z + \tilde{w} \tilde{w}_z) + \kappa T_0 \tilde{\Theta} \tilde{\Theta}_z \right] \Big|_{z=0} dx dt.
 \end{aligned}$$

2

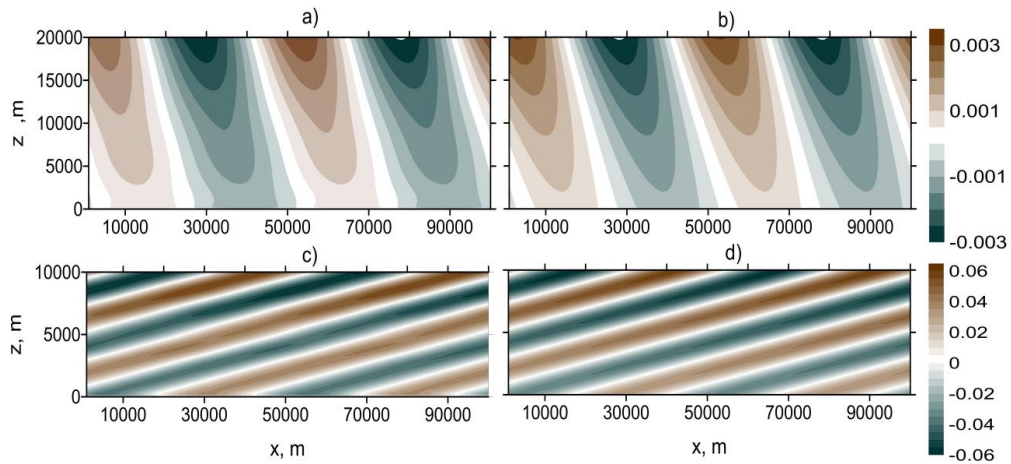
3 For the conditions (13) with the same $f_p(x, t)$ for both P_1 and P_2 , the difference $\tilde{P} = 0$ along the
 4 lower boundary $z = 0$. Then, for conditions (16), the right side integral in (A2.1) is equal to zero,
 5 hence solutions $\chi_1 \equiv \chi_2$ (similar to the Appendix A).

6

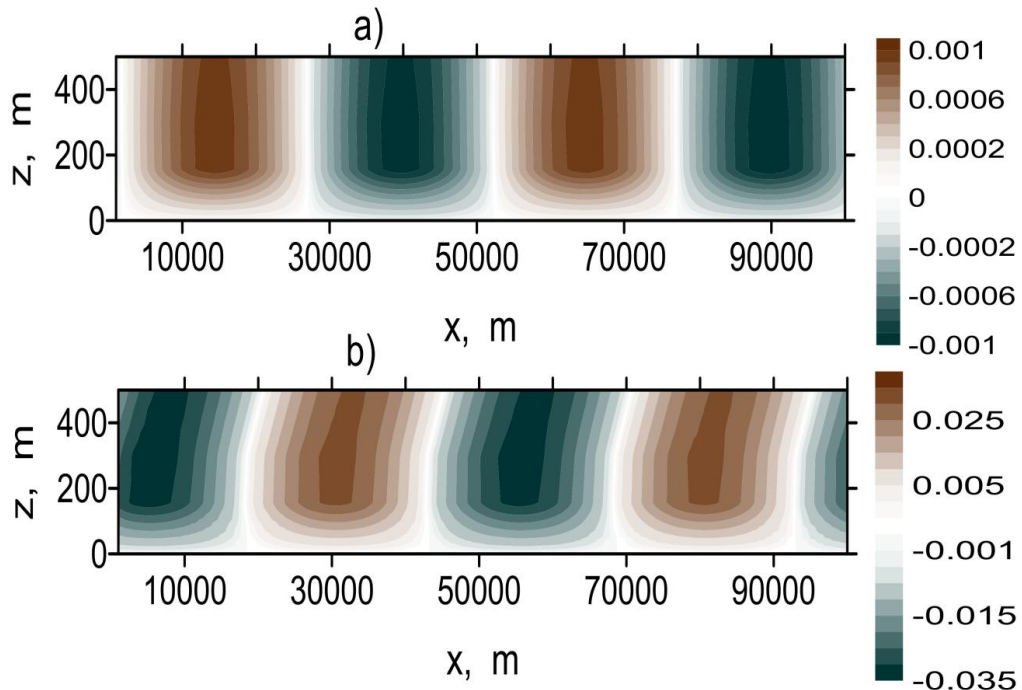
7



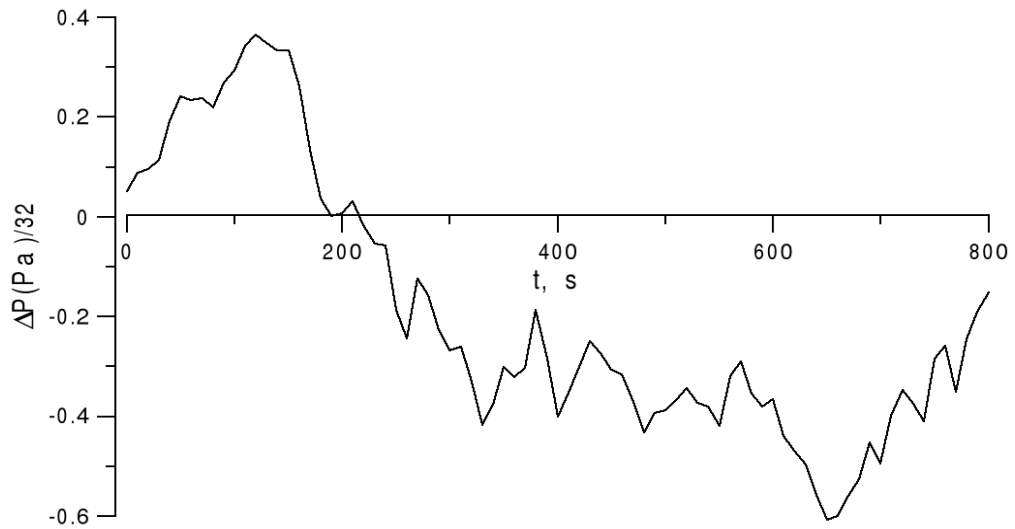
1 **Figures.**



2 **Figure 1.** Temperature perturbations in K produced by the acoustic wave at $t \approx 16$ min (top) and
3 by the internal gravity wave at $t \approx 4$ hr (bottom) simulated numerically (a, c) and calculated
4 using Eq. (18) – (20) according to the linear AGW theory (b, d).

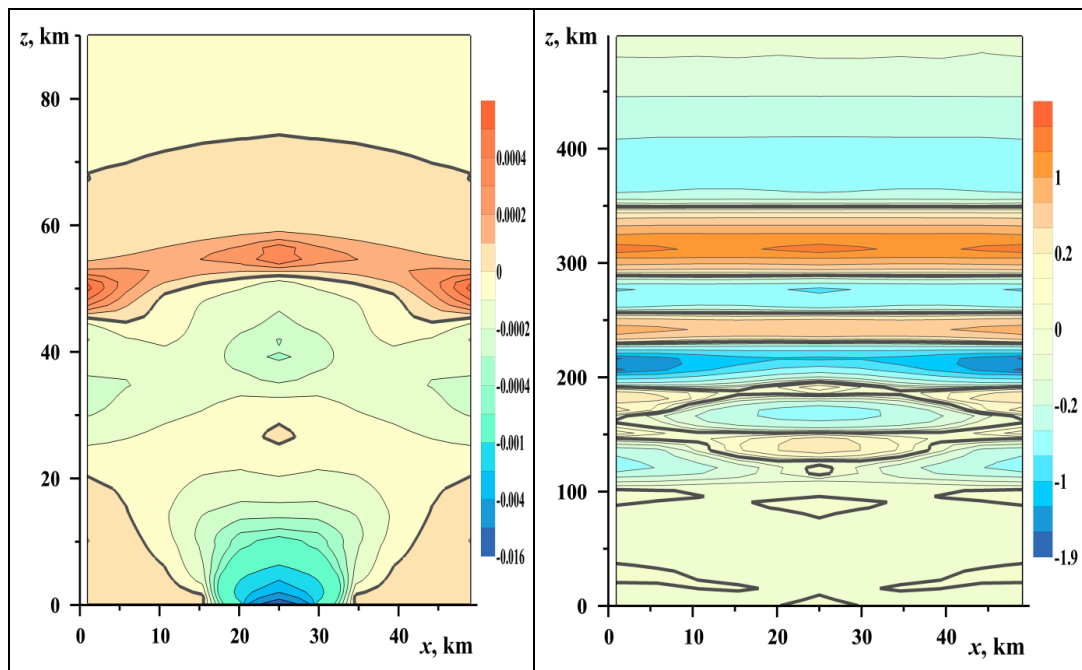


5 **Figure 2.** Simulated temperature perturbations in K near the Earth's surface produced by the
6 acoustic wave at $t \approx 16$ min (a) and by the internal gravity wave at $t \approx 4$ hr (b).



1 **Figure 3.** Surface pressure variations near Moscow on April 9, 2016.

2



3

4 **Figure 4.** Simulated temperature perturbations (in °K) due to AGWs excited by the observed
5 surface pressure variations shown in Figure 3 at $t = 3$ min (left) and $t = 13$ min (right). Thick
6 lines correspond to zero contours.